AFRL-AFOSR-VA-TR-2022-0050

Unifying Light-Induced Processes in Biology: Isomerization in Vision and Energy Transfer in Photosynthesis

Ogilvie, Jennifer
REGENTS OF THE UNIVERSITY OF MICHIGAN
503 THOMPSON ST
ANN ARBOR, MI, 48109
USA

09/30/2021
Final Technical Report

Air Force Research Laboratory
Air Force Office of Scientific Research
Arlington, Virginia 22203
Air Force Materiel Command

REPORT DOCUMENTATION PAGE

Form Approved
OMB No. 0704-0188

1. REPORT DATE *(DD-MM-YYYY)*	**2. REPORT TYPE**	**3. DATES COVERED** *(From - To)*
30-09-2021	Final	21 May 2019 - 20 May 2021

4. TITLE AND SUBTITLE
Unifying Light-Induced Processes in Biology: Isomerization in Vision and Energy Transfer in Photosynthesis

5a. CONTRACT NUMBER

5b. GRANT NUMBER
FA9550-19-1-0267

5c. PROGRAM ELEMENT NUMBER
61102F

6. AUTHOR(S)
Jennifer Ogilvie

5d. PROJECT NUMBER

5e. TASK NUMBER

5f. WORK UNIT NUMBER

7. PERFORMING ORGANIZATION NAME(S) AND ADDRESS(ES)
REGENTS OF THE UNIVERSITY OF MICHIGAN
503 THOMPSON ST
ANN ARBOR, MI 48109
USA

8. PERFORMING ORGANIZATION REPORT NUMBER

9. SPONSORING/MONITORING AGENCY NAME(S) AND ADDRESS(ES)
AF Office of Scientific Research
875 N. Randolph St. Room 3112
Arlington, VA 22203

10. SPONSOR/MONITOR'S ACRONYM(S)
AFRL/AFOSR RTB2

11. SPONSOR/MONITOR'S REPORT NUMBER(S)
AFRL-AFOSR-VA-TR-2022-0050

12. DISTRIBUTION/AVAILABILITY STATEMENT
A Distribution Unlimited: PB Public Release

13. SUPPLEMENTARY NOTES

14. ABSTRACT
Light provides a fundamental source of energy that powers a wide range of biophysical processes. In each case, light is incident upon a molecular system and is absorbed, initi- ating a sequence of subsequent molecular processes. Examples relevant to this project are animal vision, where light absorption triggers molecular isomerization followed by visual transduction leading to nerve signals in the brain, and photoinduced energy transfer, where absorbed energy is transferred to a reaction center to initiate chemical processes. Both scenarios involve light induced transport: in the first case, matter moves, in the second energy moves. Note that in all instances, and as is typical in complex biophysical processes, the nature of the environment, often the surrounding protein architecture, is important to biological function. The purpose of this high-risk high-reward project was to examine similarities and differences between these two classes of light-induced biological processes. Towards this effort, to probe the system-bath interactions relevant to this collaborative project Ogilvie developed a highly sensitive, rapid acquisition fluorescence- detected two dimensional electronic spectroscopy (FD-2DES) approach. In this approach, faster data acquisition is achieved by continuous rather than step scanning, currently enabling acquisition of FD-2DES spectra in several seconds rather than minutes. In place of a commercial lock-in amplifier, a digital acquisition board is used, enabling simultaneous collection of linear and nonlinear signals, interferometric detection of the time delays, and enhanced signal-to-noise ratios.

15. SUBJECT TERMS

16. SECURITY CLASSIFICATION OF:			**17. LIMITATION OF ABSTRACT**	**18. NUMBER OF PAGES**	**19a. NAME OF RESPONSIBLE PERSON**
a. REPORT	**b. ABSTRACT**	**c. THIS PAGE**	UU	19	SOFI BIN-SALAMON
					19b. TELEPHONE NUMBER *(Include area code)* 426-8411

Standard Form 298 (Rev.8/98)
Prescribed by ANSI Std. Z39.18

FINAL PROJECT REPORT

Unifying Light-Induced Processes in Biology: Isomerization in Vision and Energy Transfer in Photosynthesis

FA9550-19-1-0267

Program Manager: Dr. Sofi Bin-Salamon,
U.S. Air Force Office of Scientific Research

Principal Investigator: Professor Jennifer Ogilvie, Department of Physics, University of Michigan, Ann Arbor, Michigan

Co-Principal Investigator: Professor Paul Brumer, Chemical Physics Theory Group, Department of Chemistry, University of Toronto, Toronto, Ontario, Canada M5S 3H6

Light provides a fundamental source of energy that powers a wide range of biophysical processes[1]. In each case, light is incident upon a molecular system and is absorbed, initiating a sequence of subsequent molecular processes. Examples relevant to this project are animal vision, where light absorption triggers molecular isomerization followed by visual transduction leading to nerve signals in the brain, and photoinduced energy transfer, where absorbed energy is transferred to a reaction center to initiate chemical processes. Both scenarios involve light induced transport: in the first case, matter moves, in the second energy moves. Note that in all instances, and as is typical in complex biophysical processes, the nature of the environment, often the surrounding protein architecture, is important to biological function.

The purpose of this high-risk high-reward project was to examine similarities and differences between these two classes of light-induced biological processes. We note that the ongoing pandemic delayed some aspects of our work, due to increased delay times for laser repairs and reduced productivity of personnel. Nevertheless, the pandemic allowed extensive discussion between Ogilvie's and Brumer's research groups and we made significant progress as detailed below.

(i) Given our past work, and the significance of the system-environment interaction, we proposed examining, theoretically, computationally and experimentally, the possibility of extracting the spectral density $J(\omega)$ from the fluorescence Stokes shift S(t). Specifically, initial consideration was on the utility of relationship

$$J(\omega) = (\lambda/h\omega\pi)\int_0^\infty dtS(t)cos(\omega t) \tag{1}$$

that we had previously derived[2], where λ is the solvent reorganization energy. Note that the spectral density $J(\omega)$ characterizes the interaction of the system with its surroundings. The particular advantage of this expression lay in its model-and free character, under the conditions of its derivation. These include the high temperature limit of a particular two-time correlation function, and the reasonable assumption of two electronic states coupled to a gaussian environment). Our detailed theoretical studies, provided in the Appendix, showed that Eq. 1 is useful, but not model independent, for energy transfer systems, whereas it is not directly applicable for non-adiabatic dynamics, such as those in retinal in rhodopsin, whose isomerization dynamics defines the first step in vision. We have, however, obtained an extended treatment in the case of isomerization, where the spectral density is redefined to

account for interactions between the excited reactant (here cis-retinal) to the ground state product (here trans-retinal).

This analysis provides significant insight into the issue of the system-bath information content of the fluorescence Stokes shift $S(t)$ for the cases of energy transfer and isomerization in vision. Specifically, it clearly distinguishes between adiabatic energy transfer and non-adiabatic nuclear dynamics. $S(t)$ and $J(\omega)$ are functionally intertwined for adiabatic dynamics (e.g. energy transfer). but not for non-adiabatic dynamics (e.g. isomerization in vision). As noted above, an extension to isomerization dynamics is under investigation (see Appendix).

(ii) Given that the nature of the system-bath interaction is significant, Brumer's group also took an additional direction by examining the interplay between the nature of the environmentally induced decoherence (specifically, whether it is global or local) and its effect on energy transfer efficiency in a model donor-acceptor-(reaction center) system. Remarkably, we found that the effects of asymmetry (i.e. unequal excitation energies in the donor and accepter) in the dimer are generally detrimental to the transfer of energy. Four types of systems were examined, arising from combinations of localized trapping, delocalized trapping, eigenstate dephasing and site basis dephasing. In the cases of site basis dephasing the interplay between the energy gap of the excited dimer states and the environment was shown to give rise to a turnover effect in the efficiency under weak dimer coupling conditions. Furthermore, the nature of the coherences and associated flux were interpreted in terms of pathway interference effects, reminiscent of coherent control scenarios. Most significant, from the viewpoint of this research effort, is that the energy transfer efficiency was dramatically different depending on the nature of the coupling (localized or delocalized) of the system to the reaction center, a feature characteristic of the system-environment interaction. In addition, increased energy transfer was not necessarily correlated with increased coherence, in the non-equilibrium steady state relevant to natural biological processes. This work has been published in the Journal of Chemical Physics[3].

This result is of particular biophysical interest since it implies that optimal energy transfer performance would require symmetric systems, i.e. donors and acceptors of equal excitation energy. The fact that this is not the case biologically implies the role of competitive processes influencing energy transfer rates.

(iii) In an additional study, on the role of system-environment coupling in the natural-

light induced photoisomerization of retinal, Brumer's group examined a number of different models, using our newly developed methodology to compute the long-time quantum yield. Typical results for three different system-environment models are shown in Figure 2. Specifically, the ordinate is the population of the trans product as a function of time since the photoisomerization was initiated. Each of the three panels corresponds to results for different system-environment interaction, with the center panel corresponding to the usually adopted Hahn-Stock model. Two things are manifestly evident. First, the numerical values of the quantum yield, arguably the most relevant of properties in biological isomerization, is dramatically dependent on the nature of the coupling of the retinal to the environment, with quantum yield ranging in magnitude from zero to unity!. Hence, the actual value of the retinal quantum yield is highly indicative of retinal-protein interaction.

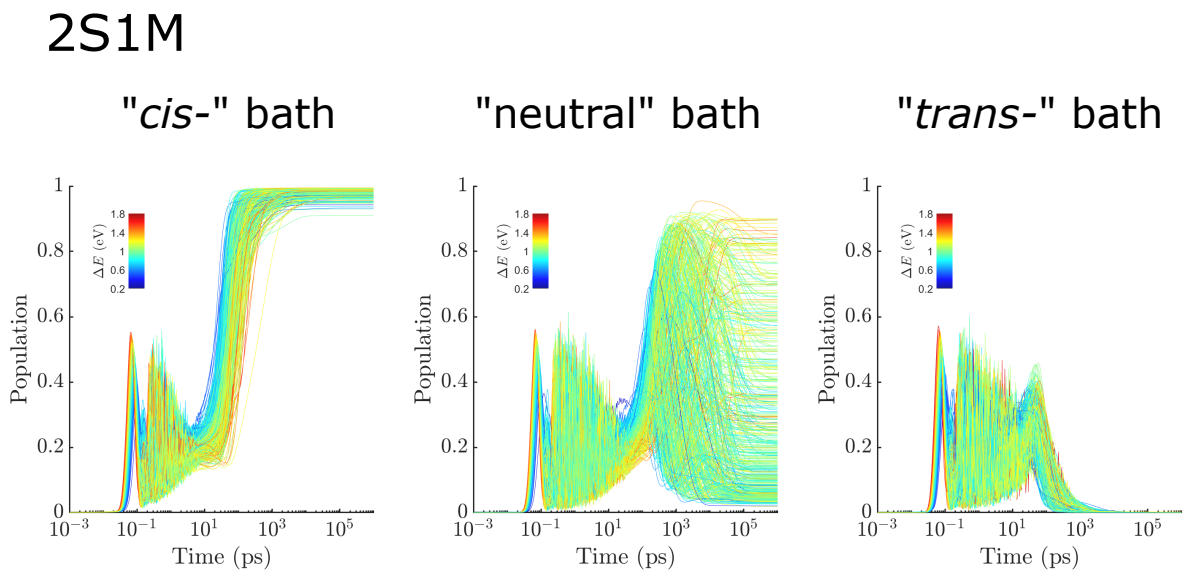

Figure 1: Quantum Yield for various system-environment models and for different optical gaps.

Second, quantum yield results are seen to vary widely within a given model. For example, in the case of the system-environment coupling in the "neutral" bath the quantum yield varies from near unity to near zero with changes in the system optical gap (here denoted ΔE). This remarkable dependence is an unexpected discovery of this work. That is, that the quantum yield, and likely other product properties, is exquisitely sensitive to system parameters. It remains to be determined, in future work, whether this behavior is parametric sensitivity associated with quantum chaos and what its role is in biology. In addition, we examined

conditions on ensemble sizes that would be necessary in order to observe this parametric sensitivity, necessary information to plan experimental studies. Results are shown in the righthand panel of Figure 2. Specifically, the black line provides a measure of the width of the distribution of quantum yields as a function of the number of molecules N in the measured ensemble. The width is largest for a single molecule, shown as the intersection with the y axis, and decreases as the inverse of the square root of N. Considering the recent advances in Ogilvie's experimental approach (described below), these results are encouraging insofar as experiments on a small sample of 1000 molecules, where parametric sensitivity would be evident, is likely feasible. These results strongly suggest the need for experimental studies on a parametric sensitivity, a study proposed as part of the focus of our future experimental-theoretical efforts. Our initial work on parametric sensitivity has been published[4].

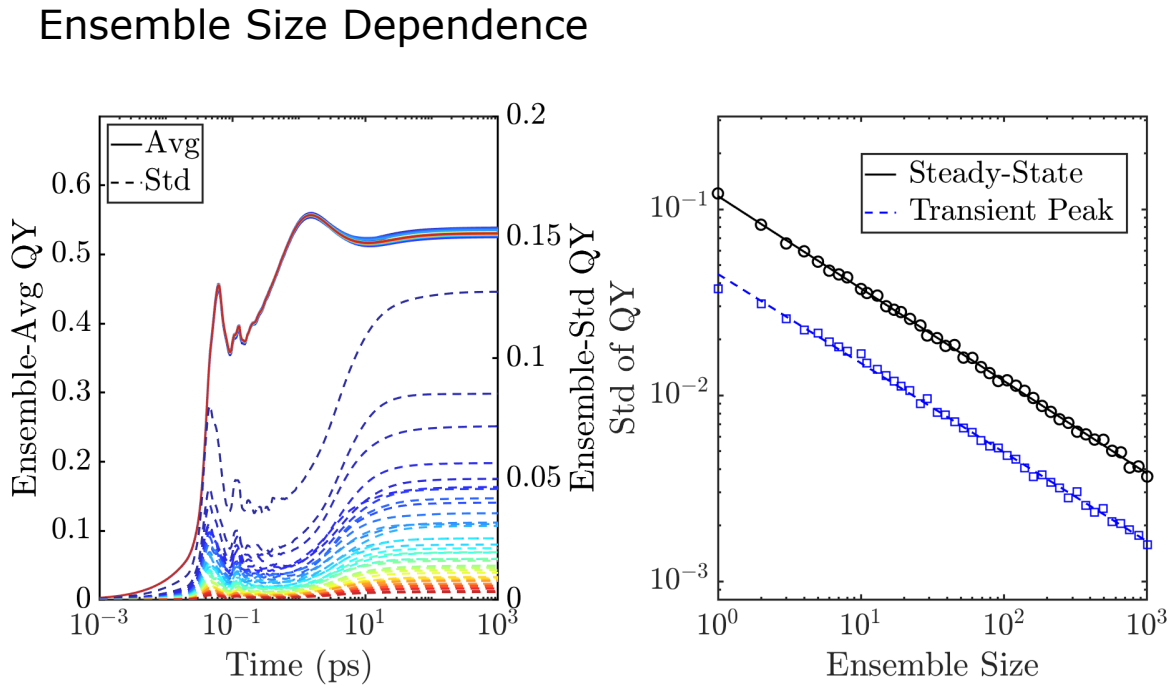

Figure 2: (Left) Time-dependence of the mean (solid) and the standard deviation (dashed) of reaction quantum yield averaged over different ensemble size. (Right) Width of the distribution of quantum yields as a function of ensemble size.

Complementary to Brumer's theoretical work, Ogilvie has made experimental progress along two important directions.

(i) To probe the system-bath interactions relevant to this collaborative project Ogilvie de-

veloped a highly sensitive, rapid acquisition fluorescence- detected two dimensional electronic spectroscopy (FD-2DES) approach. While Ogilvie has shown that the FD-2DES approach offers orders of magnitude higher sensitivity than conventional coherently-detected 2DES [5], the sensitivity and applicability of the FD-2DES approach to a broader range of systems can be further improved by reducing the overall data acquisition time, making the method less susceptible to photobleaching. Photobleaching is highly sample dependent, and remains a serious limitation for spectroscopy and imaging of biological systems. Ogilvie's original FD-2DES method used phase-modulation with AOMs and lock-in detection of the fluorescent signal. Being a Fourier-transform approach, FD-2DES employs a sequence of four laser pulses and requires the scanning of two independent time delays for the acquisition of a single FD-2DES spectrum. In Ogilvie's original implementation, lock-in detection was performed with a commercial lock-in amplifier, and the time delays were varied in discrete steps. Step-scanning increases the overall data acquisition time because the mechanical delay stages must "settle" to the desired delay prior to measurement. In addition, there can be timing errors associated with mechanical delay stages that degrades the signal-to-noise ratio of the data. The use of a conventional lock-in amplifier limits the number of independent signals that can be collected in a single scan to the number of channels on the lock-in instrument, which is typically two. Ogilvie realized that the measurements with the FD-2DES apparatus could be made an order of magnitude faster, with higher sensitivity, and could allow for parallel collection of multiple spectroscopic signals by performing signal digitization and Fourier analysis. In the new approach, faster data acquisition is achieved by continuous rather than step scanning, currently enabling acquisition of FD-2DES spectra in several seconds rather than minutes. In place of the commercial lock-in amplifier, a digital acquisition board (DAQ) with 8 input channels capable of 16 bit simultaneous acquisition at 2 MHz is used. Without the limited number of signals dictated by the commercial lock-in amplifier, additional optical signals can be recorded to enable interferometric detection of the time delays, improving the signal-to-noise ratio. In addition to the FD-2DES signals, higher order signals such as those arising from two-photon excitation can be acquired, as can lower order spectroscopic signals such as linear fluorescence excitation spectra. Remarkably, these numerous signals can be collected in a single 3 second scan and separated in the Fourier domain. The experimental setup for this new approach is shown in Figure 1. Representative data on the laser dye IR140 using the new approach is shown in Figure 2,

which illustrates the time domain signals that are simultaneously collected. Figure 3 shows the resulting complex FD-2DES spectrum. The paper reporting these results is available as arXiv:2105.13319 and has recently been accepted to the Journal of Chemical Physics Special Issue on Coherent Multidimensional Spectroscopy [6]. The significant reduction in acquisition time and improvements in sensitivity and signal-to-noise ratio represent a highly promising development for measurements at the single molecule level. Ogilvie estimates that a further enhancement of two orders of magnitude in acquisition speed could be readily achieved with faster scanning stages.

(ii) To identify unifying physical principles across light-induced biological processes it is necessary for Ogilvie to extend the capabilities of her fluorescence-detected two-dimensional spectroscopy (FD-2DES) apparatus from the near-infrared into the visible regime. The FD-2DES apparatus enables measurements of the two-time correlation function investigated theoretically by Brumer. Extending the FD-2DES apparatus to visible wavelengths requires generation of broadband visible light. Using continuum generation via tight focusing of the 1030 nm output from a 1 MHz amplified laser into a YAG disk Ogilvie produced broadband light spanning 450 -1200 nm, providing ample bandwidth for studies of bacteriorhodopsin and LH2 complexes as well as most photo-active biological systems. However, the broadband continuum is chirped, and many of the elements of the FD-2DES experiment, such as the AOMs and pulse-shaper used for dispersion compensation operate over a limited bandwidth. Ogilvie's initial plan was to build a separate FD-2DES setup to operate over limited visible wavelengths. However, during the development of the rapid-scan FD-2DES approach, Ogilvie discovered that FD-2DES spectra are relatively insensitive to the pulse chirp as shown in Figure 4. Her rapid-scan approach also provides the capability of simultaneously measuring both FD-2DES signals, as well as the amplitude and spectral phase of the exciting pulses. This opens up the exciting opportunity of post-correcting the chirp effects in FD-2DES data and obviating the need for pulse-compression entirely. A demonstration of the ability to post-correct the FD-2DES data is in progress. This discovery has opened up the possibility of modifying the existing FD-2DES setup to enable measurements spanning 450 - 1200nm, the largest bandwidth to date for multidimensional spectroscopy measurements. This advance is particularly exciting because it would enable the simultaneous study of one and two photon transitions, as well as coupling and energy transfer dynamics over an unprecedented spectral range. Key to demonstrating this advance it to

perform the phase-modulation step prior to continuum generation. This work is also in progress in Ogilvie's lab and can be extended to coherently-detected 2DES and sensitive linear absorption measurements of nonfluorescent species.

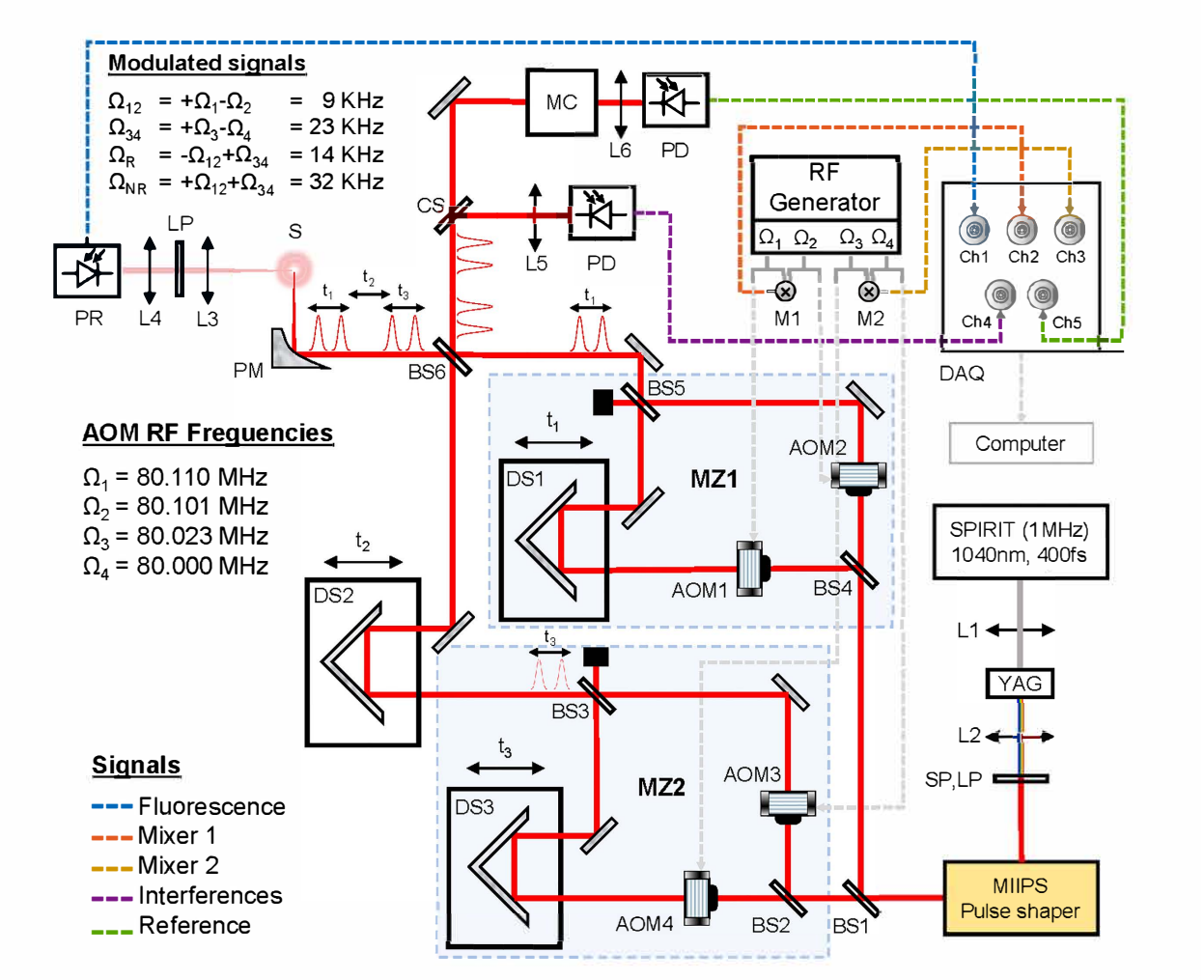

Figure 3: Experimental setup of the rapid-scanning phase-modulated fluorescence-detected 2D spectrometer (FD-2DES). Beamsplitter (BS), Acousto-Optic Modulator (AOM), Mach-Zehnder interferometer (MZ), Monochromator (MC), Photodiode (PD), Variable Gain Photoreceiver (PR), Shortpass Optical Filter (SP), Longpass Optical Filter (LP), Cover Slip (CS), Lens (L), Sample (S), Parabolic Mirror (PM), Data acquisition card (DAQ).

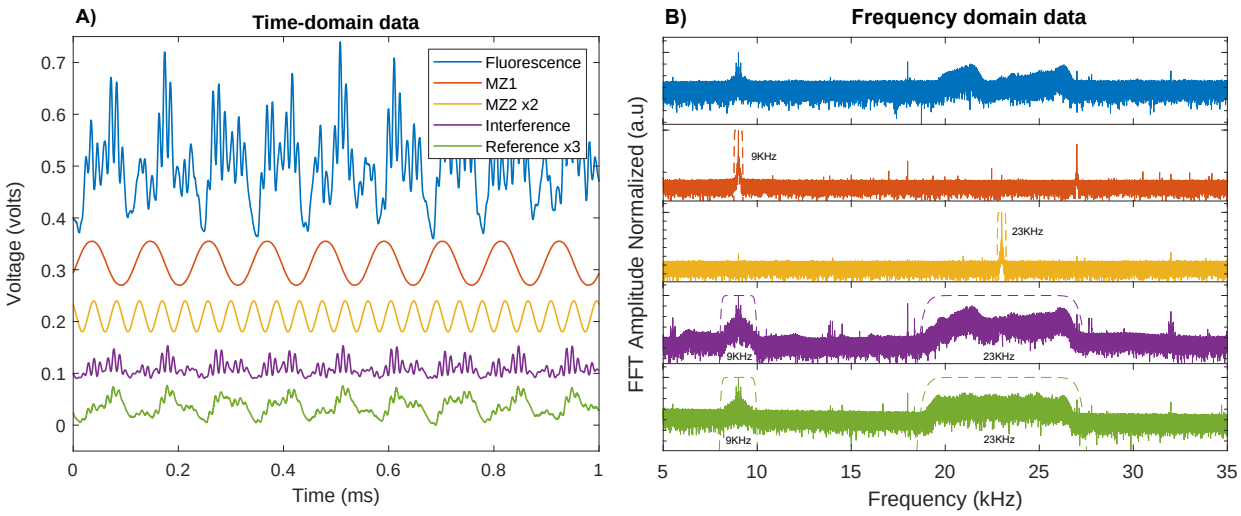

Figure 4: A: Digitized time domain signals for interferometric simultaneous detection of FD-2DES and linear fluorescence excitation spectra. B: The Fourier transform of the time domain signals shown in panel A reveal unique frequencies that enable separation of multiple nonlinear spectroscopic signals of interest.

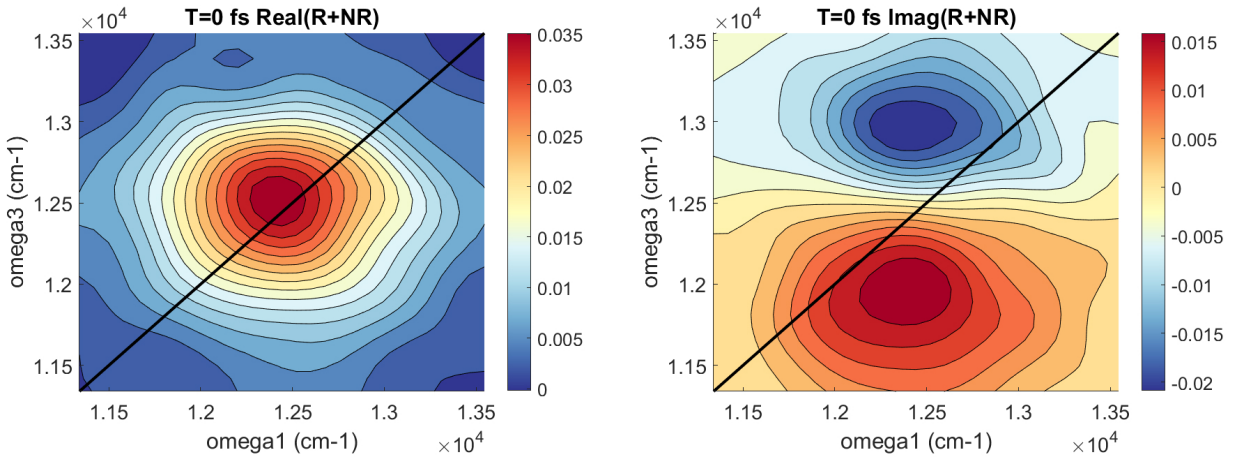

Figure 5: Real (left) and imaginary (right) FD-2DES spectra at T=0 from the laser dye IR140. The data was acquired in a 3 second scan.

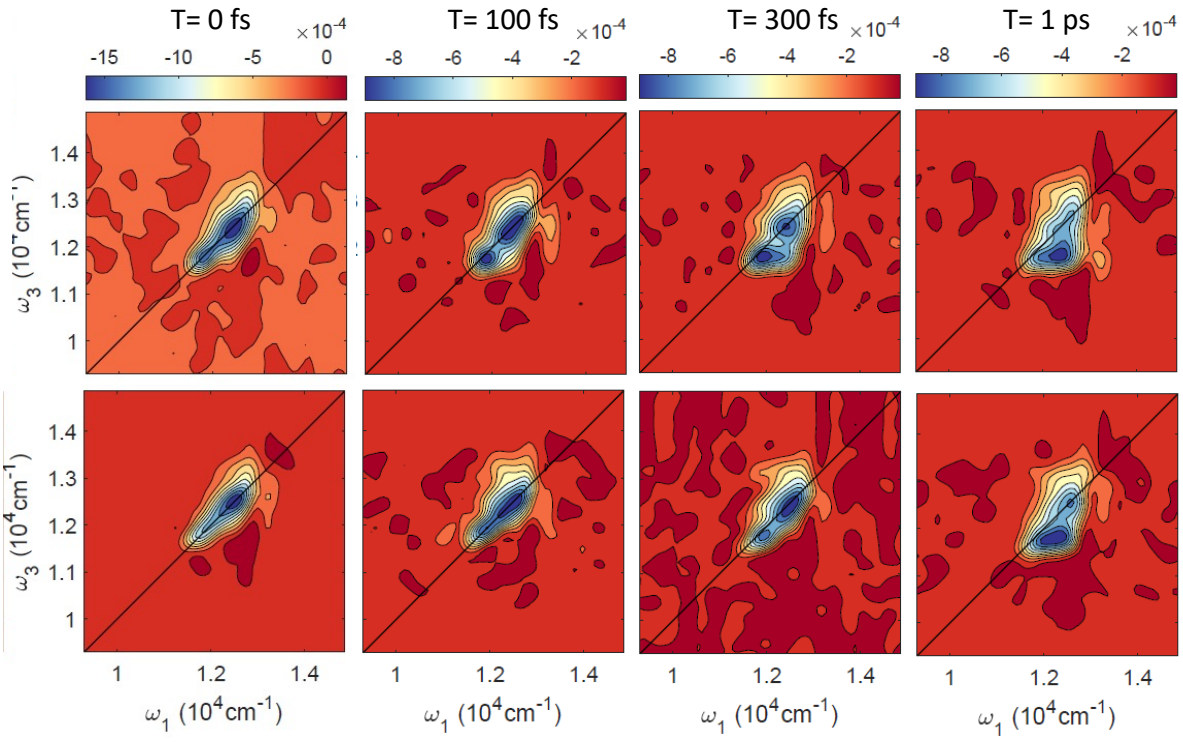

Figure 6: Top row: FD-2DES spectra at different waiting times for IR144 in DMSO using transform-limited pulses. Bottom Row: FD-2DES spectra at different waiting times for IR144 in DMSO using pulses with $3000 fs^2$ chirp, showing a weak dependence of the FD-2DES spectra on pulse chirp.

Appendix: Developments in the relation of the Fluorescence Stokes Shift and the Spectral Density

I. $S(t)$ FOR SINGLE LEVELS

Note: The notation in this document is made to be consistent with that of Ref. 7.

The fluorescence Stokes shift (FSS) is defined by

$$S^{\text{noneq}}(t) = \frac{U(t) - U(\infty)}{U(0) - U(\infty)}, \tag{2}$$

where $U(t)$ is the difference of the excited state and ground state at time t due to the effect of a laser pulse. The superscript denotes that this is a nonequilibrium response. This nonequilibrium response be related approximately to an equilibrium response function through the use of linear response theory and the Condon approximation.[8, 9] The result is

$$S^{\text{noneq}}(t) \approx S^{\text{eq}}(t) = \frac{\langle \rho_g U(t) U(0) \rangle}{\langle \rho_g U^2(0) \rangle} = \frac{C(t)}{C(0)}, \tag{3}$$

which relies on the classical limit of the linear response formalism.[10]

To relate the definition in Eq. (3) to the spectral density the correlation function function, $C(t)$, must be examined in closer detail. To do this $C(t)$ will be split into its real and imaginary parts

$$C(t) = C'(t) + iC''(t), \tag{4}$$

where

$$C'(t) = \frac{1}{2\hbar} \left[\langle \rho_g U(t) U(0) \rangle + \langle \rho_g U(0) U(t) \rangle \right], \tag{5}$$

and

$$C''(t) = \frac{-i}{2\hbar} \left[\langle \rho_g U(t) U(0) \rangle - \langle \rho_g U(0) U(t) \rangle \right]. \tag{6}$$

In the Fourier domain it can be shown that Eq. (4) can be written as[7]

$$\tilde{C}(\omega) = \tilde{C}'(\omega) + \tilde{C}''(\omega), \tag{7}$$

with

$$\tilde{C}'(\omega) = 2 \int_0^\infty d\omega \cos(\omega t) C'(t), \tag{8}$$

and

$$\tilde{C}''(\omega) = 2\int_0^\infty d\omega \sin(\omega t) C'(t). \tag{9}$$

An important relationship between the real and imaginary parts is given by

$$\tilde{C}'(\omega) = \coth(\beta\hbar\omega/2)\tilde{C}''(\omega). \tag{10}$$

For harmonic baths (which will be assumed throughout this document) $\tilde{C}''(\omega)$ is temperature independent and contains all information of the bath. This defines $\tilde{C}''(\omega)$ as the spectral density.[7]

Following Ref. 7, chapter 8 it can be shown that one can relate Eq. (5) to the spectral density via

$$\frac{C'(t)}{C'(0)} = \frac{1}{\pi\Delta^2}\int_0^\infty d\omega \tilde{C}''(\omega)\coth(\beta\hbar\omega/2)\cos(\omega t), \tag{11}$$

where

$$\Delta^2 = \frac{1}{\pi}\int_0^\infty d\omega \tilde{C}''(\omega)\coth(\beta\hbar\omega/2). \tag{12}$$

To obtain a relationship between Eq. (3), which is a classical correlation function, and Eq. (11), which is quantum, one must look in the limit as $\beta \to 0$ i.e. the high temperature limit. In this limit:

$$\lim_{\beta\to 0}\Delta^2 = \frac{2}{\beta\pi\hbar}\int_0^\infty d\omega \frac{\tilde{C}''(\omega)}{\omega} = \frac{2\lambda}{\beta\hbar}, \tag{13}$$

and from Eq. (5)

$$\lim_{\beta\to 0} C'(t) = C(t) \tag{14}$$

giving

$$\lim_{\beta\to 0}\frac{C'(t)}{C'(0)} = \frac{C(t)}{C(0)} = S^{\mathrm{eq}}(t) = \frac{1}{\pi\lambda}\int_0^\infty d\omega \frac{\tilde{C}''(\omega)}{\omega}\cos(\omega t), \tag{15}$$

which is a relationship between the spectral density and the FSS. One can redefine the spectral density, as

$$J(\omega) = \frac{1}{\pi\hbar}\frac{C''(\omega)}{\omega^2}, \tag{16}$$

and substitute this expression into Eq. (15) to give

$$S^{\mathrm{eq}}(t) = \frac{\hbar}{\lambda}\int_0^\infty d\omega\ \omega J(\omega)\cos(\omega t), \tag{17}$$

which is the desired result.

To briefly recap, the approximations made to get to Eq. (17) rely on the high temperature (classical) limit of $C(t)$, linear response theory (which relates $C(t)$ to the FSS in the Condon limit) and a two-level system Hamiltonian coupled to a gaussian environment. These

approximations amount to a classical relationship between the FSS and the spectral density which will limit the amount of information that can be ascertained. Namely, all effects that would be considered quantum mechanical in nature due to system-bath entanglement will be absent in the obtained spectral density from Eq. (17).

II. MULTI-LEVEL SYSTEMS

The case for multi-level spin systems is complicated by the correlation between the system and the bath. To illustrate this issue, it is helpful to recast the above discussion into a simple picture of classical mechanics.

A. Classical Picture of Electronic Gap Dynamics for Single Level Systems

Consider the simplest case of a shifted harmonic oscillator model:

$$H = |g\rangle\langle g| + |e\rangle\langle e| \cdot \left(U_0 - \sum_k d_k \omega_k^2 x_k + \lambda \right) + \sum_k \frac{\omega_k^2}{2} x_k^2 + T \tag{18}$$

where $\lambda = \sum_k d_k^2 \omega_k^2 / 2$. Essentially this is two electronic, multi-dimensional quadratic surfaces, shifted in each direction by d_k with respect to one another.

At the start of dynamics, the system is prepared to be in the Franck-Condon state on the upper surface. Assuming that all modes are frozen at the origin with zero thermal energies, for each of the mode one recovers a simple harmonic motion with frequency ω_k and magnitude d_k, $x_k(t) = d_k(1 - \cos \omega_k t)$. Hence the energy gap as a function of time reads

$$U(t) = U_0 + 2 \cdot \sum_k \frac{\omega_k^2 d_k^2}{2} \cos(\omega_k t) \tag{19}$$

The factor of two accounts for the corresponding variation of energy in the lower surface. This is the same expression as Eq. (17), by defining the spectral density function $J(\omega) = \pi \sum_k d_k^2 \omega_k \delta(\omega - \omega_k)/2$ and changing to the integral expression.

B. Multi-level Systems, Incoherent Dynamics

For a generic multi-level system coupled to independent baths in the site basis, we have:

$$H = H_{\rm s} + H_{\rm b} + H_{\rm sb} \tag{20}$$

$$H_{\rm s} = \sum_n U_n |n\rangle\langle n| + \sum_{n,m} J_{n,m} |n\rangle\langle m| \tag{21}$$

$$H_{\rm sb} = \sum_{n,k} \left(-d_{n,k}\omega_{n,k}^2 x_{n,k} + \lambda_n\right) |n\rangle\langle n| \tag{22}$$

The system is diagonalized by its eigenstates $H_{\rm s}|s\rangle = U_s|s\rangle$, where $|s\rangle = \sum_n c_n^s |n\rangle$ and c_n^s is the wavefunction magnitude on site n. The above picture cannot be applied here, since in general coherence between different levels (sites) prohibits simple definitions of classical surfaces.

A zeroth order approximation to this situation is to simply ignore the inter-site coherences and assume that the system state is describable by a incoherent mixture of site populations at all times. In this sense each site evolves on its own multi-dimensional surface independently, weighted by the population.

$$U_s(t) = U_s(0) + \sum_n P_n(t) \sum_k \omega_{n,k}^2 d_{n,k}^2 \cos(\omega_{n,k} t) \tag{23}$$

Notice that even in this drastically simplified case, there is no direct way of inverting the gap dynamics and retrieving the bath spectral densities $J_n(\omega)$. Not only one needs to take into account the population transfer dynamics among the sites, $P_n(t)$, but also the local characters of the baths, that in general $J_n(\omega) \neq J_m(\omega)$ for different sites $n \neq m$. Numerically modelling the dynamics with different initial conditions is the only course possible.

C. Multi-level Systems: System-bath Correlation

In general, the relaxation of individual site baths renormalizes the system itself and correlates the system dynamics with those of the baths, which is not taken into account in the above mentioned picture. Thus, the electronic eigenstates of the system are subject to the influence of the bath dynamics.

In our simplified picture, this amounts to introduce time dependence of the electronic gap $U_0 = U_0(t)$, assuming the adiabatic limit. The system dynamics operates on a renormalized Hamiltonian as the system-bath correlation builds up.

A particularly illuminating example is to consider the long-time limit where the system and bath composite is allowed to fully equilibrate. In this case, one recovers the steady state limit of the fluorescence emission, given by

$$\langle s|E(t)|s\rangle = \langle s|\mathrm{Tr}_\mathrm{b}\left(\hat{\mu}(t)\hat{\mu}\rho^\mathrm{eq}\right)|s\rangle \tag{24}$$

where $\hat{\mu} = \sum_n |0\rangle\langle n| + \mathrm{H.c.}$ is the transition dipole operator and $\rho^\mathrm{eq} = \mathrm{Tr}_\mathrm{b} e^{-\beta H}/Z$ is the equilibrium reduced density matrix with $Z = \mathrm{Tr} e^{-\beta H}$. [11] The frequency dependent spectrum is obtained by the half-sided Fourier transform of $E(t)$.

Due to the finite system-bath coupling, ρ^eq is in general not diagonal in the system eigenbasis (Boltzmann state). It turns out one can employ a high temperature approximation and resum the matrix exponential.[12] The result writes

$$\rho^\mathrm{eq} \approx \frac{1}{Z^\mathrm{eff}} e^{-\beta H_\mathrm{s}^\mathrm{eff}} \tag{25}$$

$$H_\mathrm{s}^\mathrm{eff} = \hat{U} - \hat{\Lambda} + e^{-a\beta\hat{\Lambda}}\hat{J}e^{-a\beta\hat{\Lambda}} \tag{26}$$

where $\hat{U}$ and $\hat{J}$ are the diagonal and the off-diagonal part of H_s, respectively. $\hat{\Lambda} = \sum_n \lambda_n |n\rangle\langle n|$ and $a = 1/6$. Essentially, this states that the thermal state is characterized by an effective Hamiltonian with on-site energies $U_n^\mathrm{eff} = U_n - \lambda_n$ and couplings $J_{nm}^\mathrm{eff} = J_{nm} e^{-a\beta(\lambda_n+\lambda_m)}$.

Assuming the adiabatic limit, that the renormalization process is slow and does not induce inter-level transfer, this redefines the long-time limit of the energy gap:

$$U_s(t\to\infty) \approx \langle s'|H_\mathrm{s}^\mathrm{eff}|s'\rangle \tag{27}$$

where $|s'\rangle$ is the eigenstate of $H_\mathrm{s}^\mathrm{eff}$ corresponding to $|s\rangle$ of H_s.

1. *Numerical Evaluation of $S(t)$*

While the long-time limit of $U(t)$ is bounded by Eq. (25), the generic dynamics is subjected to initial conditions. To properly account for the correlated system-bath dynamics, one requires methodologies that treat the system-bath coupling nonpertubatively and beyond the Born approximation. One such method is the hierarchical equations of motion (HEOM).[13]

To retrieve $S(t)$, we return to Eq. (24) and replace the equilibrium reduced density matrix by its time-dependent counterpart $\rho(t)$ with certain initial condition $\rho(0)$. This corresponds

to a pump-probe measurement, and the dynamical Stokes shift can be obtained by isolating the stimulated emission pathways therein. [13] The overall process is repeated by comparing the resulting $S(t)$ to that experimentally measured.

2. Theoretical Development

Depending on the parameter regime such as the strength of the system-bath coupling and temperature relative to the system energy scale, the fitting procedure involving HEOM can be numerically challenging, as significant memory is required to converge the hierarchy and properly describe the system-bath correlation.

One possible way to lessen the numerical effort is to recognize that the renormalization of thermal state is described by a single parameter $a = 1/6$, and the initial state can be understood as setting $a = 0$. Thus, it is suggestive to assume a time dependent profile $a = a(t)$ that scales between the two limits. Thus, instead of propagating in the imaginary time axis $t = -i\tau$, one attempts to resum the real time propagator $G(t) = \mathrm{Tr_b} e^{-iHt}$, or the dynamical mapping in the field of quantum process tomography.

III. NONADIABATIC SYSTEMS: RETINAL PHOTOISOMERIZATION

All of the above discussions assume the adiabatic approximation, that the electronic state involved has a continuous character throughout the dynamics. It is under this assumption that one can define the thermal state $\rho^{\mathrm{eq}} = e^{-\beta H}/Z$ to be entirely in the singly excited state manifold. And it is from there one measures the emission of a photon concerted with the relaxation back to the electronic ground state and reveals information of the spectral density.

For nonadiabatic photo-induced processes this picture cannot be applied. For example, the photoisomerization of retinal in opsin protein pockets involves vibronic relaxation that takes the initial wavepacket back to the ground state. Thus, the separation of time scales (emission lifetime being much larger than the vibrational relaxation in the electronic excited state) does not apply in this case, and therefore the ill-definition of ρ^{eq}. It is for this reason the above discussed procedure of extracting $J(\omega)$ from $S(t)$ is not an option for retinal systems.

However, a different aspect of bath information can indeed be extracted in a similar fashion, albeit using a different experimental setup. Here we propose to use the so-called pump-dump-probe experiment[14] and extract the spectral density that measures the shifts of equilibrium positions between those in the *cis*- and the *trans*-wells.

Specifically, we start by defining the model Hamiltonian.

$$H_{\rm s} = \sum_{n,n'=0,1} \left[\left(E_n + (-1)^n \frac{V_n}{2}(1-\cos\phi) + \kappa x \delta_{n,1} \right) \delta_{n,n'} + \lambda x (1-\delta_{n,n'}) \right] |n\rangle\langle n'| + \frac{\omega x^2}{2} + \hat{T} \tag{28}$$

$$H_{\rm sb} = -\sum_k \left(\mathcal{P}_{cis} |1\rangle\langle 1| d_k^{1,c} + \mathcal{P}_{trans} |1\rangle\langle 1| d_k^{1,t} + \mathcal{P}_{trans} |0\rangle\langle 0| d_k^{0,t} \right) \cdot \omega_k^2 x_k + \hat{\Lambda} \tag{29}$$

where we adopt the two-state-two-mode (2S2M) model proposed by Stock et al.[15] as a minimal model to describe the photoisomerization reaction of retinal rhodopsin. It is composed of two diabatic electronic states $|0\rangle$ and $|1\rangle$, a reaction coordinate ϕ, and a harmonic tuning mode x. The nonadiabatic coupling term λx is needed to account for the conical intersection bridging the two surfaces. We define the region $-90^\circ \leq \phi < 90^\circ$ to be *cis*-conformer and correspondingly the projection operator $\mathcal{P}_{cis}$. Similarly $90^\circ \leq \phi < 270^\circ$ defines a *trans*-conformer and $\mathcal{P}_{trans}$.

The form of Eq. (29) implies that except for the shifts in the equilibrium positions, the frequencies of all the vibrational modes remain unchanged regardless of the system coordinates, *i.e.* no Duschinsky's rotation. The equilibrium positions, however, are shifted with respect to the overall ground state *cis*-well on diabatic state $|0\rangle$. The spectral densities corresponding to the terms $d_k^{1,c}$ ($J^c(\omega) = \pi \sum_k (d_k^{1,c})^2 \omega_k \delta(\omega - \omega_k)/2$) and $d_k^{0,t} - d_k^{1,t}$ ($J^t(\omega) = \pi \sum_k (d_k^{0,t} - d_k^{1,t})^2 \omega_k \delta(\omega - \omega_k)/2$) are in a sense the usual spectral densities: They describe the shift of the equilibrium position on the upper surface with respect to the lower surface for each mode.

More interestingly, the spectral density $J^{ct}(\omega) = \pi \sum_k (d_k^{1,t})^2 \omega_k \delta(\omega - \omega_k)/2$ describes the relative shift of the modes in the *trans*-well with respect to the *cis*. Noting that in the context of most if not all retinal systems, the two wells are separated by a significant energy barrier (≈2 eV for rhodopsin), in which thermally activated crossing happens on a time scale much longer than the bath reorganization processes. This allows a similar treatment of the bath relaxation dynamics of a vibronic wavepacket initially prepared in the equilibrium positions of the *cis*-well, relaxes into the new equilibrium positions of the *trans*-well. Such

a dynamical process can be described by Eq. (17) in principle, since a thermal state in the *trans*-well can be properly defined, $\rho^{\rm eq} = e^{-\beta H^{trans}}/Z$.

The above mentioned relaxation process can be monitored by a pump-dump-probe experimental setup. The essential difference is that the first two pulses prepare the nonequilibrium state in the $trans-$well and one measures the absorption of photons by the *trans*-wavepacket to its upper surface. This is in contrast to the fluorescence emission as in the previous cases. Here we assume that within the time interval between the pump and the dump pulses all the bath coordinates remain in their equilibrium positions in the *cis*-well. This is justified for systems like retinal rhodopsin, where it is estimated that the vibronic wavepacket traverses to the *trans*-region in less than 100 fs. [16] Aligning the time delay between the pump and the dump pulses to match this time scale, the delay time between the probe and the dump pulses provides a dynamical sketch of the vibrational relaxation in the *trans*-well, with its long-time limit defined by the *trans*-conformer absorption spectrum. Also, notice that the optical gap function $U(t)$ in this case conveys the information of the "direct product" between the spectral densities $J^{ct}(\omega)$ and $J^{t}(\omega)$.

---

[1] S. Johnsen, *The Optics of Life: A Biologist's Guide to Light in Nature* (Princeton University Press, 2011).

[2] L. Pachon and P. Brumer, J. Chem. Phys. **141**, 174102 (2014).

[3] K. Jung and P. Brumer, J. Chem. Phys. **153**, 114102 (2020).

[4] C. Chuang and P. Brumer, J. Phys. Chem. Lett. **12**, 3618 (2021).

[5] V. Tiwari, Y. A. Matutes, A. T. Gardiner, T. L. C. Jansen, R. J. Cogdell, and J. P. Ogilvie, Nat. Commun. **9** (2018).

[6] D. Agathangelou, A. Javed, F. Sessa, X. Solinas, M. Joffre, and J. P. Ogilvie, J. Chem. Phys. (accepted for publication) (2021).

[7] S. Mukamel, *Principles of Nonlinear Optical Spectroscopy* (Oxford University Press, 1995).

[8] M. Maroncelli and G. R. Fleming, J. Chem. Phys. **89**, 5044 (1988).

[9] M. Maroncelli, J. Chem. Phys. **94**, 2084 (1991).

[10] D. Chandler, *Introduction to Modern Statistical Mechanics* (Oxford University Press, 1987).

[11] J. Ma and J. Cao, J. Chem. Phys. **142**, 094106 (2015).

[12] A. Gelzinis and L. Valkunas, J. Chem. Phys. **152**, 051103 (2020).

[13] L. Chen, R. Zheng, Q. Shi, and Y. Yan, J. Chem. Phys. **132**, 024505 (2010).

[14] A. Rupenyan, I. H. M. van Stokkum, J. C. Arents, R. van Grondelle, K. J. Hellingwerf, and M. L. Groot, J. Phys. Chem. B **113**, 16251 (2009).

[15] S. Hahn and G. Stock, J. Phys. Chem. B **104**, 1146 (2000).

[16] P. J. Johnson, M. H. Farag, A. Halpin, T. Morizumi, V. I. Prokhorenko, J. Knoester, T. L. Jansen, O. P. Ernst, and R. D. Miller, J. Phys. Chem. B **121**, 4040 (2017).